TECHNICAL REPORT

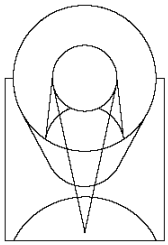

SPACE TELESCOPE SCIENCE INSTITUTE
Operated for NASA by AURA

Title: A library of simulated cosmic ray events impacting JWST HgCdTe detectors.	Doc #: JWST-STScI-001928, SM-12 Date: December 2, 2009 Rev: -
Authors: M. Robberto Phone: 410-338-4382	Release Date: March 9, 2010

1.0 Abstract

I present a library of simulated cosmic ray events on JWST HgCdTe detectors. The cosmic rays are calculated for different levels of solar activity, taking into account the relative frequency of the most abundant nucleons (H, He, C, N, O, Fe) and their energy. A shielding of 100mil Al equivalent thickness is assumed. The cosmic rays are traced through the detector material assuming they impact a random point within a pixel and are isotropically distributed. The energy losses are calculated using state of the art modeling for the different detector material, taking into account the stoichiometric ratio and density of HgCdTe and assuming optimal detector thickness. The effect of interpixel capacitance is finally added to the charges generated by the cosmic rays through convolution with a coupling filter function.

2.0 Introduction

The effect of cosmic rays (CR) on JWST detectors has always been a primary concern. In an early analysis of the broader issue of CR damage on the critical spacecraft components and materials, Barth & Isaacs (1999) assumed the radiation exposure resulting for a nominal five-year mission at the Earth-Sun L2 Point, with launch date in June 2009. Using these same assumptions, Rauscher et al. (2000) presented a specific study of the effects of CRs on JWST detectors, discussing the advantages and limitations of the various readout modes (double correlated sampling, Fowler,…) in dealing with CRs. Rauscher et al. (2000) assumed InSb detectors with 27 micron pixel pitch.

The main goal of this paper is to revisit this issue building a library of realistic CR impacts that may be added to the simulation of raw data taken by JWST detectors in order to optimize the data reduction processing. With respect to to Rauscher et al. (2000) the main change is the modeling of CR impacts of HgCdTe detectors, taking into account the correct stoichiometry, density and the best available information on the detector geometry (thickness). The result is a set of fits files containing a collection of CRs which

should be representative of the relative frequency of the impacting nucleons (I include H, He, C, N, O and Fe), their energy, impact direction and detector parameters.

3.0 Tutorial on the JWST radiation environment

This section is intended as a tutorial on the JWST radiation environment and therefore can be skipped by readers familiar e.g. with the Barth & Isaacs (1999) paper.

In general, it is customary to distinguish between two types of cosmic ray radiation:
"transient" particles, typically protons and heavier nucleons of all elements of the periodic table;
particles trapped by the Van Allen belt. These include protons, electrons and heavier nucleons.

The cosmic ray flux at L2 is basically composed by transient particles. Only during the transfer trajectory on its way to L2 JWST will encounter trapped particles. Since the detectors will not take science data in these early phases one can from now on ignore trapped particles (this paper does not deal with the issue of possible CR induced damages on the detector material).

Among the transient particles, one can distinguish between two basic types: galactic (a term used regardless on their real galactic or extragalactic origin; one should probably better say "non-solar") particles and solar particles. Both types are generally assumed to be isotropic, to the first order.

1) Galactic cosmic rays are mostly composed by protons (85%) and He (13%), with energy ranging from ~1MeV to several TeV. These are the highest energy particles, dominating the spectrum above ~50 MeV/nucleon.

2) The solar particles have lower energy and are strongly modulated by the Sun's activity. Low energy particles have the largest cross-section and therefore are primary sources of CR events on the detectors. On the other hand, they can be efficiently shielded (see below) and therefore one sees only the high energy tail of their distribution. The main contribution comes from protons accelerated by solar flares which may occur several times a day over a period of several hours. However, during the periods of solar maxima one has the much more severe coronal eruptions (coronal arcs), which typically occur ~10 times per year over a period of several days. Eruptions deliver energetic protons, alpha particles, heavy ions, and electrons with energies up to 100's MeV, or in the GeV range for the heavier ions. Their estimated typical fluxes are about 2000 particles/cm^2/s, i.e. hundreds of times larger than the other components. It is safe to assume that under these solar storms the detectors will not take data; however, one still can include them in the simulations as they represent our worse case scenario.
It must be reminded that the solar activity shows significant variation cycle-to-cycle, and therefore predictions relative to the future cycles are extremely uncertain. Figure 1 (from http://www.swpc.noaa.gov/SolarCycle/index.html) illustrates how the number of

sunspots, a classic indicator of solar activity, varied during the last four cycles and the range of variability expected for the coming cycle, of interest for JWST.

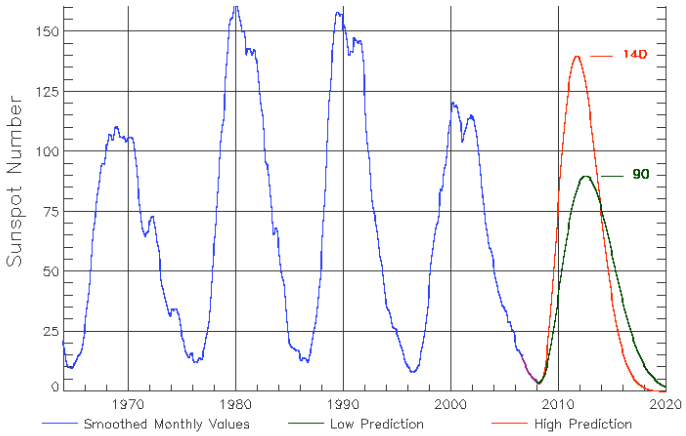

Figure 1: recent history of solar activity and current predictions for the coming cycle.

The galactic and solar components are not independent. The solar activity modulates the flux of galactic cosmic rays, establishing (especially at lower energies) an anti-correlation between the fluxes of galactic and solar radiation. This will be made clear in Section 4.0. Previous JWST studies (Barth 2000, Fodness 2002) assume a shielding of 100 mils of Al. As already mentioned, this substantially mitigates the low energy component, i.e. typically the solar one. Shielding, on the other hand, has negligible impact on the high energy particles.
For completeness, one must mention two other components of cosmic rays:

3) the Anomalous Cosmic Rays (ACRs), first discovered in 1973 as a "bump" in the spectra of certain elements (He, N, O, Ne, and later H, Ar, and C) at relatively low energies (~10MeV/nucleon). ACRs arise primarily from neutral interstellar atoms swept into the solar cavity by the motion of the Sun through the interstellar medium. Measurements to date indicate that trapped ACRs have steep spectra and are therefore unlikely to be a significant radiation hazard for systems shilded by ~50mil Al equivalent, or more (see https://creme96.nrl.navy.mil/cm/ACR.htm).

4) the solar wind ("low energy plasma", Barth & Isaacs 1999), composed by low energy (few eV) electrons, protons and ions is technically speaking part of the radiation environment. However, it can be easily shielded and therefore will be neglected hereafter. Besides the primary CR particles, secondary particles are produced through the spacecraft shielding and may contribute to the ionization environment. CR protons hitting a nucleus may generate secondary electrons (delta-electrons) or activate the nucleus, which subsequently may decay producing particles like the quark-antiquark combinations known as π mesons. This second channel is especially interesting, since the π^0 mainly decays in two gamma photons, whereas the $\pi^{\pm}$ decay in $\mu^{\pm}$ muons and neutrinos. At the

Earth surface, most of the CR flux is degraded into muons, which are therefore the main cause of "real" CR events on CCDs on the ground. In this study these events are neglected, relying on the basic assumption that most of the energy is lost through proton-electron anelastic scattering. In any case, it may be appropriate to underline that the electron/holes generated by CR events inside the detectors, which represent the focus of this study, can be fully regarded as part of the family of secondary CR particles.

4.0 Cosmic Ray Spectrum

The CREME96 model (https://creme96.nrl.navy.mil/) has been used to predict the cosmic ray fluence on JWST. CREME96 is based on two main modules:

a) The CREME96 FLUX module provides a numerical model of the space ionizing-radiation environment at the surface of the spacecraft, ***before*** transport through shielding.

b) The CREME96 TRANS module. After running FLUX for the environment and orbit in which one is interested, one can run the TRANS program to transport the particle fluxes through the assumed shielding.

For the FLUX module three scenarios have been assumed:

Case 1) Solar minimum – Galactic maximum.
Case 2) Solar maximum – Galactic minimum
Case 3) Solar flare

I have not considered trapped particles, irrelevant for a L2 orbit, whereas anomalous cosmic rays are included in the CREME96 model. The solar flare has been averaged over the worst week, which corresponds to a period of over the 180 hours (=7.5 days) beginning at 13:00 UT on 19 October 1989. This was the most severe environment observed in the two recent strong solar maxima (roughly 1980.5-83.5 and 1989.0-92.0) and can be regarded as a "99% worst case" environment for systems designed to operate through solar maximum.
The fluence, for all elements up to z=92, has been calculated before and after the nominal JWST shielding of 100mil Al equivalent. The results are presented in Figure 2.
The rise at low energy is due to solar particles, whereas the main "bump" is due to galactic particles. The figures clearly show how the shielding depresses the low energy spectrum (left vs. right column), and how during the solar flares the galactic component becomes negligible, overwhelmed by the flare.
The dominant contributors to the CR fluence are mostly H and He, followed by C, N, O and Fe. This paper is therefore limited to these elements only. Electrons, neutrons, and gamma-rays are *not* included in the CREME96 FLUX models. In general, electrons and gamma rays are not expected to be a significant cause of single event effects. Neutrons are absent from galactic cosmic rays and relatively rare in solar particle events. Neutrons, however, can be *locally* produced by nuclear interactions of cosmic rays in thick shielding. These secondary neutrons may cause damage to the material and possibly dominate the total dose accumulated by instrumentation (and crews!) living under thick-shielding during a long-duration mission. However, they do not lose energy interacting

with the electrons. In any case, the present version of CREME96 TRANS (which transports particle fluxes through shielding) does not track neutrons.

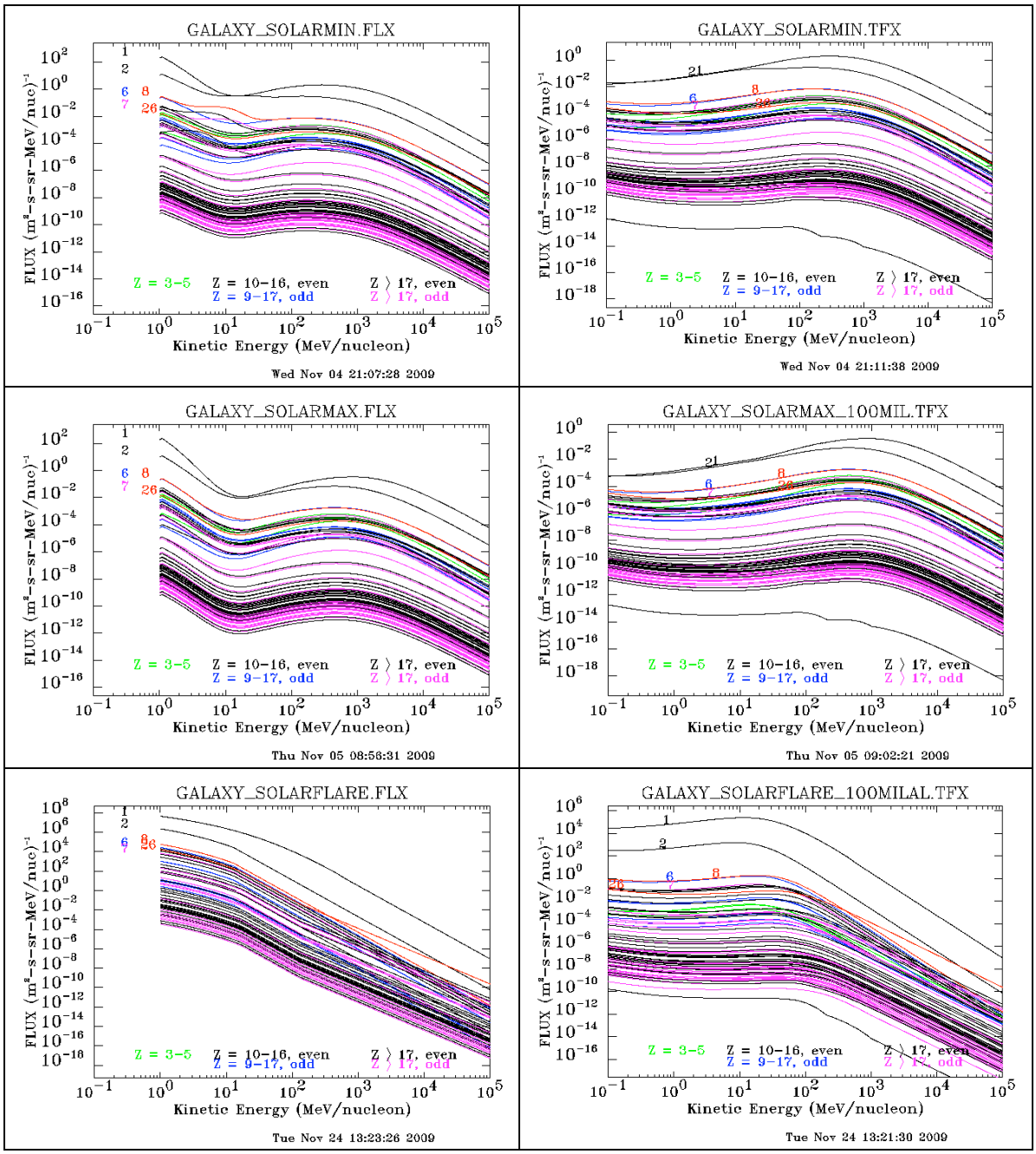

Figure 2: flux of cosmic rays in the 3 cases considered: solar minimum (top row), solar maximum (middle row) and solar flare (bottom row). The left column refers to the flux predicted in the interplanetary space, without shielding, whereas the right column refers to the flux predicted after 100Al equivalent shielding.

To illustrate more clearly the situation, Figure 3 shows a zoom-in of Figure 2 with the fluxes of the 6 most abundant ions. It is now evident that the galactic component drops at the solar maximum, "pushed away" by the solar flux. The solar flux, however, is not really seen by the detector being well shielded. Therefore, during a solar quiet period the CR fluency is actually lower at solar maximum rather than at solar minimum.

The situation is very different when solar flares occur: the CR flux becomes higher by 3 orders of magnitudes, after 100mil Al equivalent shielding. This is an extreme case which may possibly never appear in the JWST lifetime, as it represents an historic peak. Also, it seems reasonable to assume that under extreme solar flares the instruments will not take data, similarly to what happens when the HST crosses the South Atlantic Anomaly. The case of a strong solar flare in our model mostly for reasons of completeness.

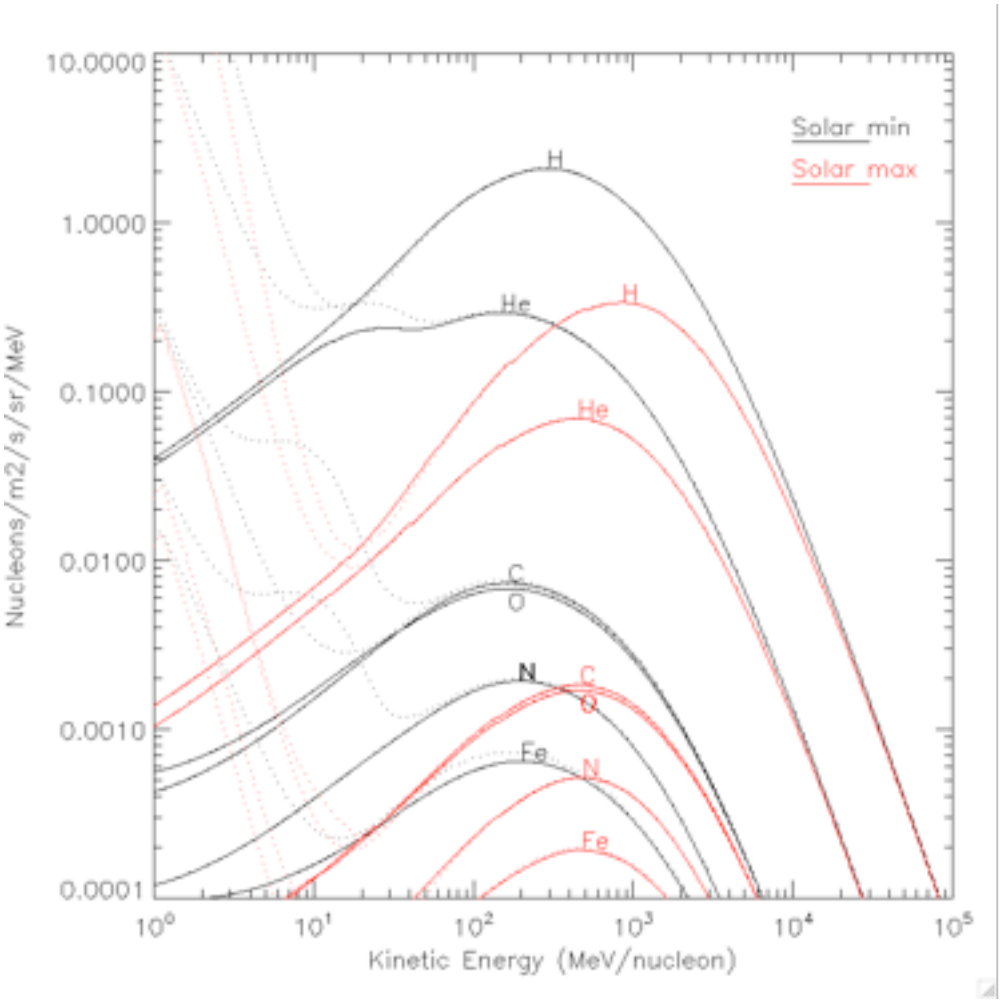

Figure 3: Similar to Figure 2, relative only to the 5 most abundant nucleons (H, He, C, O Fe) for both solar minimum and solar maximum conditions.

Table 1 shows the integrated fluxes, in nucleons/cm2/s, for the 6 cases considered. The events/cm2/s commonly assumed for JWST. As shown in Table 1, this is composed by a 91.1% of protons and 8.4% of helium, with the other elements contributing for the residual 0.5% of events.

This flux decreases by a factor of 3 at solar maximum but increases up to a factor 1500 during solar flares (worse case scenario).

Table 1 Integrated fluence of CR

		No shield		100mil Al shield	
		Flux	**fraction**	**Flux**	**fraction**
Solar Minimum	H	*13.9405*	*0.9339*	*4.4626*	*0.9111*
	He	*0.9364*	*0.0627*	*0.4106*	*0.0838*
	C	*0.0216*	*0.0014*	*0.0108*	*0.0022*
	N	*0.0042*	*0.0003*	*0.0029*	*0.0006*
	O	*0.0221*	*0.0015*	*0.0103*	*0.0021*
	Fe	*0.0018*	*0.0001*	*0.0011*	*0.0002*
	Total	***14.9266***		***4.8983***	
Solar Maximum	H	*10.3846*	*0.9366*	*1.5782*	*0.8875*
	He	*0.6691*	*0.0603*	*0.1882*	*0.1058*
	C	*0.0148*	*0.0013*	*0.0051*	*0.0029*
	N	*0.0025*	*0.0002*	*0.0014*	*0.0008*
	O	*0.0151*	*0.0014*	*0.0048*	*0.0027*
	Fe	*0.0012*	*0.0001*	*0.0006*	*0.0003*
	Total	***11.0873***		***1.7783***	
Solar Flare	H	*2168686*	*0.9497*	*3033.4*	*0.9956*
	He	*109855.0*	*0.0481*	*13.300*	*0.0044*
	C	*1281.10*	*0.0006*	*0.0422*	*0.0000*
	N	*378.360*	*0.0002*	*0.0093*	*0.0000*
	O	*2722.90*	*0.0012*	*0.0664*	*0.0000*
	Fe	*731.400*	*0.0003*	*0.0112*	*0.0000*
	Total	***2283654.76***		***3046.83***	

A final notice on the multiplication factors:

- The area of the JWST HgCdTe detectors is 18micron × 2048^2 = 13.5895 cm^2.
- The minimum readout time is (at the moment) t=10.6 seconds.

The average number of CR per read is therefore, at solar minimum:

$$N = 4.8983 \times 13.5895 \times 10.6 = 705.59 \text{ CRevent/read.} \quad (1.1)$$

For the computation, a MonteCarlo method has been implemented to randomly generate a) the type of nucleon and b) its energy after 100mil Al equivalent shielding according to the distributions presented above.

5.0 Energy loss by CRs

When a high-energy massive charged particle travels through the matter it loses energy. At the typical energy of CRs (<100GeV) the energy is mostly lost through inelastic collisions with the bound electrons of the material. The mean energy loss (-dE/dx) is therefore calculated by summing the contributions of all possible scatterings. The calculation of the cross sections are performed using different approximations appropriate for different values of the kinetic energy of the scattered electrons. To an accuracy of a few percent over a wide range of energies one can use the classic *Bethe-Bloch* formula (Amsler et al. 2008):

$$-\frac{dE}{dx} = Kz^2 \frac{Z}{A}\frac{1}{\beta^2}\left[\frac{1}{2}\ln\left(\frac{2m_e c^2\beta^2\gamma^2 T_{\max}}{I^2} - \beta^2 - \frac{\delta(\beta\gamma)}{2}\right)\right] \qquad (1.2)$$

where $\frac{dE}{dx}$ is in units of Mev/cm, $K = 0.307075$ Mev/g/cm2, z is the charge of the incident particle (i.e. $z = 1$ for a proton), Z and A are the atomic number and mass (in g/mol) of the absorber, β and γ are the usual relativistic factors for the incident particle, $T_{\max}$ is the maximum kinetic energy which can be imparted to a free electron in a single collision and I is the mean excitation energy in eV. The last term in parenthesis represents a density-effect correction: the electric field produced by the incident particle becomes depressed at large distances because the material gets polarized. This truncates the logarithmic rise in the formula.

The Bethe-Bloch formula allows to calculate the amount of energy lost by a charged particle (including muons and pions) crossing a material characterized by a small set of parameters, the most uncertain being the mean excitation energy I . In Figure 4 the Bethe-Bloch formula (without the density-effect correction) is used to evaluate the amount of energy lost by CR in HgCdTe with cutoff at 5.5micron. The target properties are fully derived in the next section, whereas the expression of $T_{\max}$ is taken from Eq. (27.2) of Amsler et al. (2008).

The *Bragg curve* represents the energy lost by a particle traveling through matter, and is therefore specific to an incident particle of given initial energy. For a slow (1MeV) proton in HgCdTe material with cutoff at 5.5micron, one obtains for example the curve shown in Figure 5. It shows that a 1MeV proton is completely stopped after about 20 micron of material.

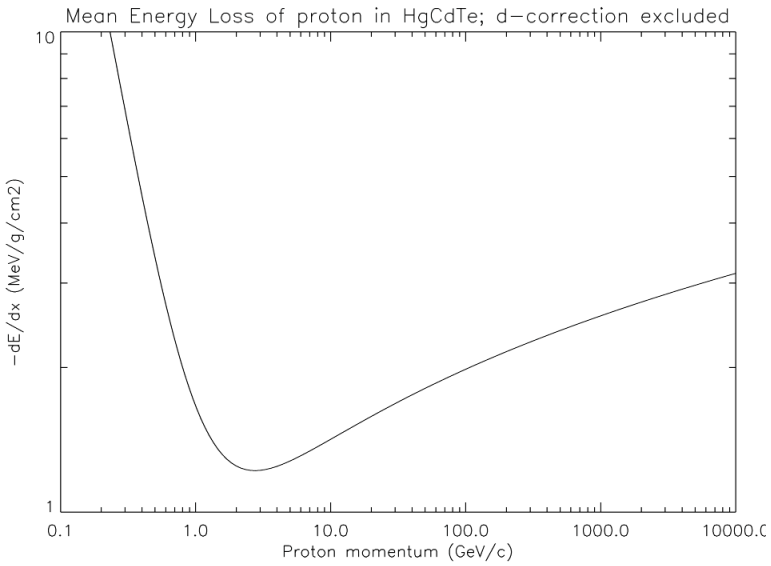

Figure 4: Energy losses of protons in HgCdTe material with cutoff at 5.5micron, predicted by the Bethe-Bloch equations (without density correction)

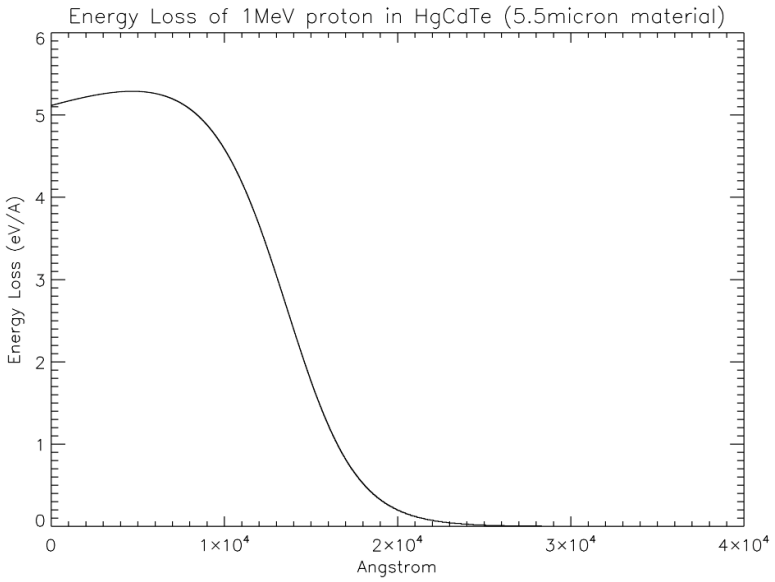

Figure 5: Bragg curve for a 1MeV proton in HgCdTe with 5.5micron cutoff, based on the Bethe-Bloch equation represented in Figure 4.

It is possible to perform more detailed calculations of the energy losses in the target material, in our case HgCdTe, using numerical models. In particular, SRIM (Stopping and Range of Ions in Matter), available at http://www.srim.org/, is a software tool which allows to calculate the stopping and range of ions (up to 2 GeV/amu) into matter using a full quantum mechanical treatment of the ion-atom collisions. SRIM accepts unconventional target materials, such as HgCdTe, and therefore provides results more

robust against the uncertainties in the parameters of the material, such as the mean excitation energy I .
Before discussing the results obtained with SRIM, it is necessary to specify the main properties of the HgCdTe.

5.1 HgCdTe properties

For an alloy like HgCdTe, the SRIM code requires to specify 3 basic parameters:

1. stoichiometric ratio
2. density
3. thickness

These parameters depend on the cutoff wavelength of the detector.

5.2 Stoichimetric ratio

The wavelength of the bandgap $E_g(\text{eV})$ of the HgCdTe material can be tuned by varying the fractional composition (stoichiometric ratio) x of Cd vs. Hg, thanks to the fact that the semimetal HgTe has (at 77 K) $E_g = -0.26$ eV whereas the semiconductor CdTe has $E_g = 1.6$ eV (also at 77K).

Following Hansen and Schmit (1983), the bandgap of the $Hg_{1-x}Cd_xTe$ alloy is given by the formula

$$E_g(\text{eV}) = -0.302 + 1.93x + 5.35\times10^{-4}T(1-2x) - 0.810x^2 + 0.832x^3 \quad (1.3)$$

and therefore depends on the composition as well as on the temperature. One can assume three cases, corresponding to three different types of detectors produced by Teledyne and of interest for the JWST project:

- A 5.5micron cutoff material designed to operate at T=35K
- A 2.5micron cutoff material designed to operate at T=77K
- A 1.75micron cutoff material designed to operate at T=150K

The first two materials are those actually used in JWST, whereas the third one is used in the WFC3 IR detector flying on the HST, which can be used for comparison with real data. The design temperatures listed above may be different from the actual operation temperatures. In particular, for the 5.5 detectors of JWST operated at about 37K and the 1.7 micron detector in WFC3 operated at 145K the difference is small. For the 2.5micron detector instead one can assume the standard LN2 temperature, which represents the usual operating temperature of 2.5micron detectors. This is based on the assumption that Teledyne has followed the standard and most reliable material growth recipe, optimized for 2.5micron detectors working at 77K.
With these assumptions it is, remembering that $E(\text{eV}) = hc/\lambda(\mu\text{m}) = 1.24/\lambda(\mu\text{m})$:

- $x_{5.5} = 0.295$
- $x_{2.5} = 0.458$
- $x_{1.75} = 0.588$

Note that we are neglecting the impurities added to create the PN junction in the bulk material.

5.3 Density

It is known that the density of HgCdTe depends on the stoichiometric ratio. Following Capper (1994, and references therein), one can use the relation

$$\rho = 8.076 - 2.23x(\pm 0.02) \quad \text{g cm}^{-3} \qquad (1.4)$$

which translates in the following values:

- $\rho_{5.5} = 7.418$
- $\rho_{2.5} = 7.055$
- $\rho_{1.75} = 6.765$.

5.4 Thickness

HgCdTe detectors are grown with MBE technique on a thick ZnCdTe substrate. The substrate is removed in the late stages of production, leaving only the thin layer of HgCdTe sensitive to the incoming photons. There is an optimal thickness for the HgCdTe photosensitive layer, driven by the absorption depth of IR photons in the material. The chart presented in Figure 6, available on the public domain, illustrates the "rule of thumb" that supposedly has been adopted by Teledyne: the thickness of the active layer is equal to the cutoff wavelength. It is, therefore:

- $d_{5.5} = 5.5 \quad \mu\text{m}$
- $d_{2.2} = 2.2 \quad \mu\text{m}$
- $d_{1.75} = 1.75 \quad \mu\text{m}$.

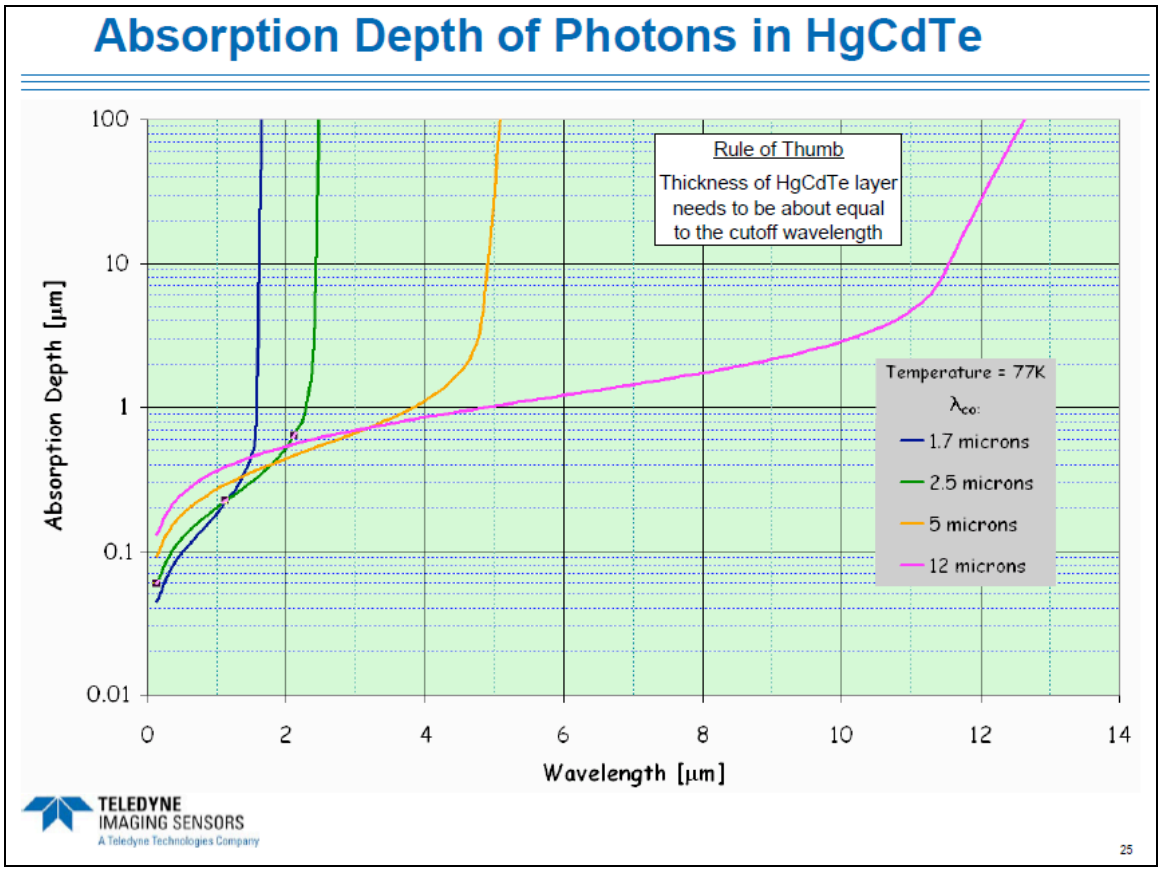

Figure 6: Recipe for optimal thickness of HgCdTe detectors. From http://www.ppdd.final.gov/eppoffice-w/Research_Techniques_Seminar/Talks/beletic.pdf

6.0 Energy loss by CRs: detailed calculation.

Having defined the properties of the material, one can use SRIM, in particular the module TRIM (Transport of Ions in Matter) to calculate the final 3D distribution of the ions in the material, together with the kinetic phenomena associated with the ion's energy loss: target damage, sputtering, phonon production and, most important in our case, ionization. Figure 7 shows a screen capture of the main TRIM window. It is relative to a 1MeV proton (parameters in ION DATA) impacting a HgCdTe alloy of 5.5micron thickness optimized for 5.5micron cutoff wavelength (the density and stoichiometry being defined accordingly).

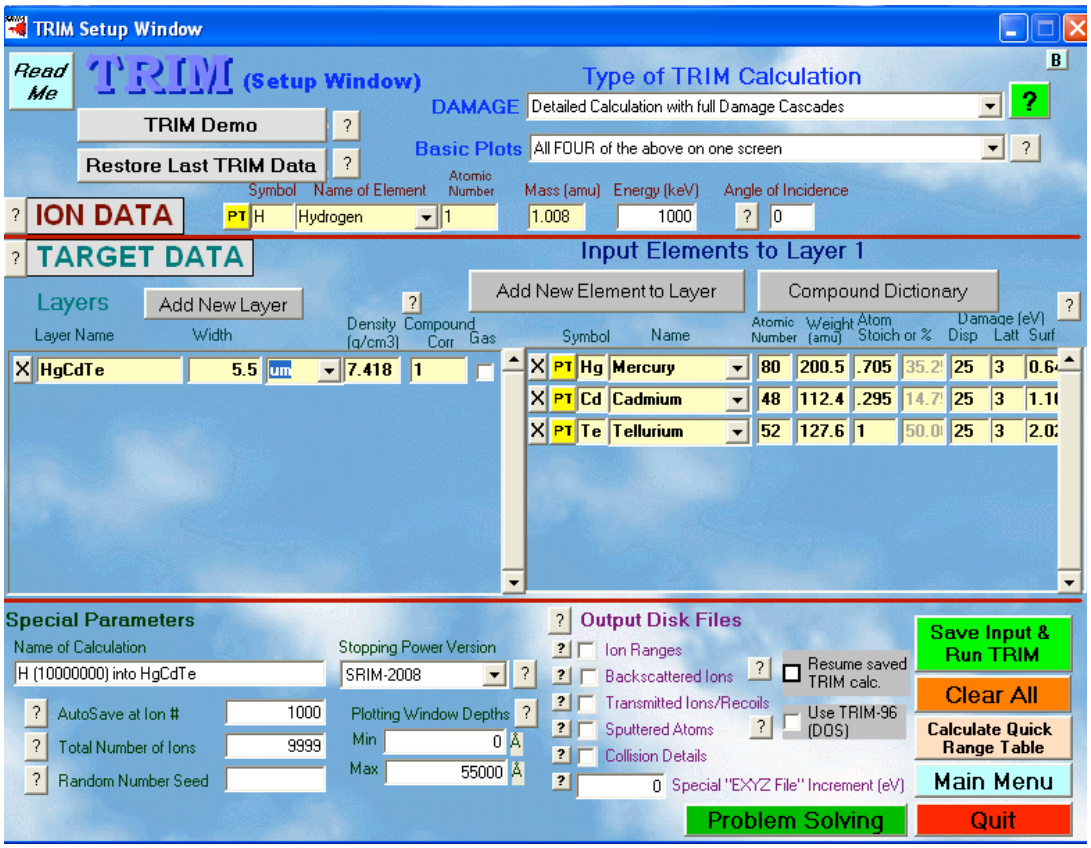

Figure 7: screen capture of the TRIM input window for a 1MeV proton impacting 5.5micron of HgCdTe material optimized for a cutoff at 5.5micron.

Figures 8 and 9 illustrate the results obtained for protons (Figure 8) and Helium ions (Figure 9) impacting the 5.5micron HgCdTe. The left columns show the Bragg curve, which is particularly clear in Figure 9 top-left (1MeV Helium atom), with a morphology very similar to the one presented in Figure 5. The corresponding figure for a proton (Figure 8 top-left) can be directly compared with Figure 5. If one refers to the entry point of the 1MeV proton in the material, the Bethe-Bloch equation provides a loss of 5.1eV/A vs. a value closer to 5.5eV/A calculated by TRIM, i.e. the Bethe-Bloch equation is correct within 10%, as expected at these energies.

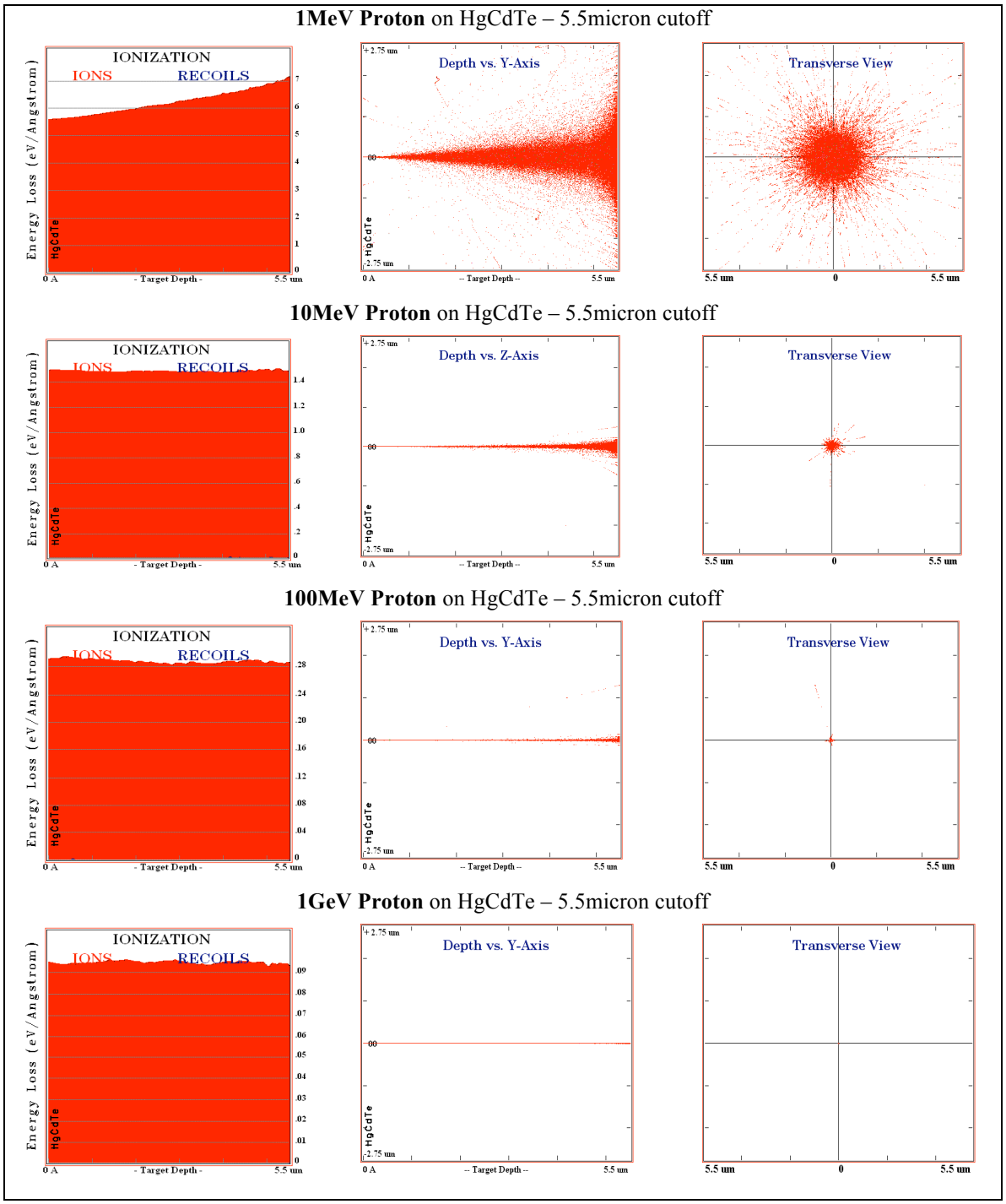

Figure 8: TRIM Results for protons of different energy (from top to bottom: 1MeV, 10MeV, 100MeV, 1GeV) impacting on 5.5micron HgCdTe. The left column shows the energy loss (Bragg curve), the central column shows a longitudinal view with generated charges, the right column shows the transverse view of the generated charges.

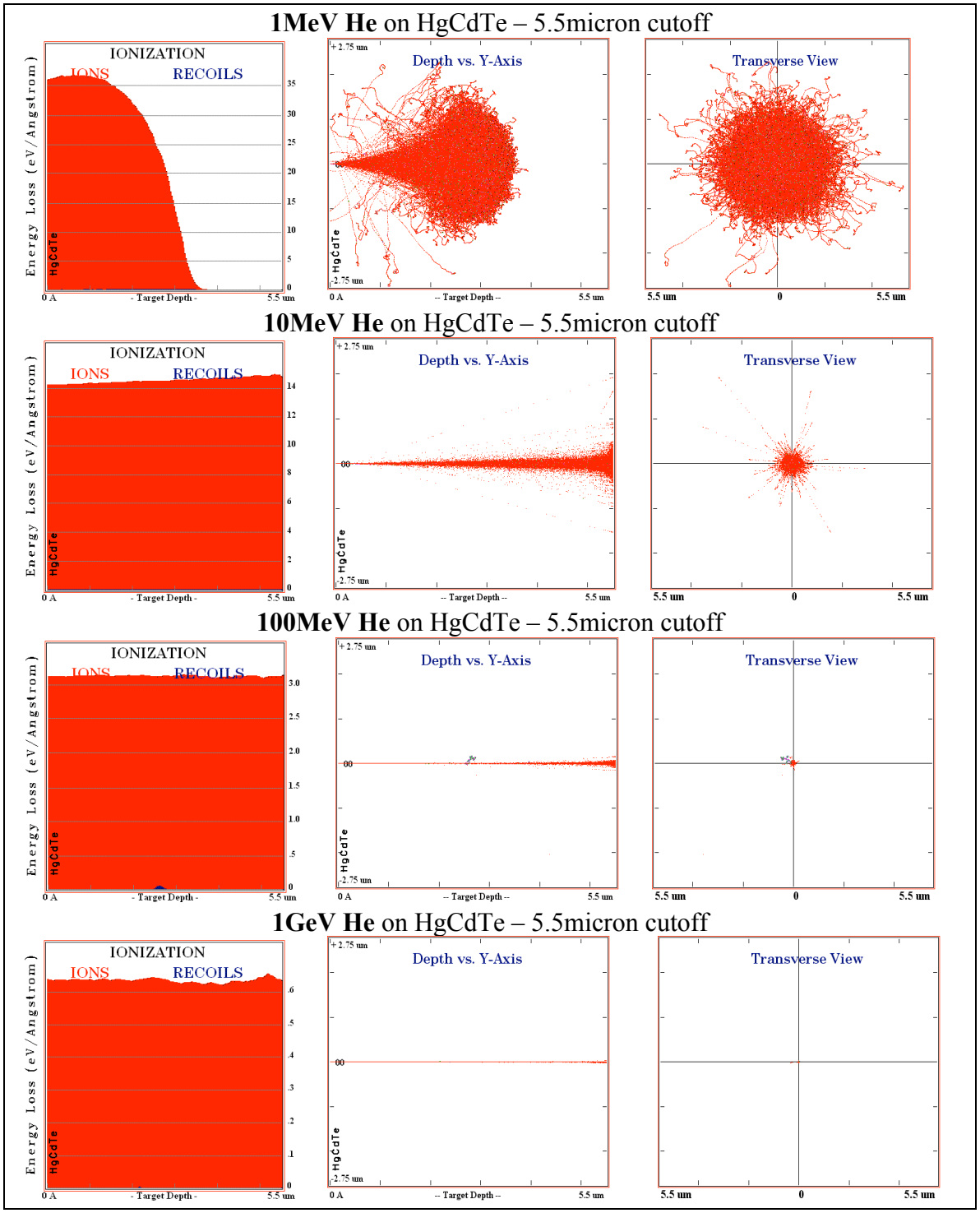

Figure 9: similar to Figure 8 for He ions on 5.5 HgCdTe

An important result that one can derive from these plot is that even for the heavy ions (such as Helium) of lowest energy the ionization cloud remains well confined within a few microns from the particle track. This allows to assume a simple geometric model where the pixels interested by the CR events are those directly crossed by the particle.

The SRIM code allows extracting the Energy losses represented in Figure 8 and 9 in tabular form. These are the tables used in the last steps of the simulation.

7.0 CR generation on HgCdTe detectors

Knowing the energy spectrum (after 100mil Al equivalent shielding) and losses of H, He, C, N, O and Fe nucleons impacting HgCdTe material of different composition, one has all the ingredients to generate CR traces inside the detector and derive the amount of generated charge.

This last step only requires basic geometry. The code assumes square pixels 18micron ×18micron size, with thickness corresponding to the cutoff wavelength according to the prescription presented in Section 5.3. It calculated the electrons released by a CR over a 21 × 21 pixel region of the detector, large enough to account for nearly tangential events and interpixel coupling of the most violent events. The CRs are assumed entering a random point within the central pixel (10,10), with a random angle over 4pi steradiants. Effects like charge creation in the detector Silicon multiplexer or secondary particles are neglected.

The calculation, performed in IDL, estimates the length of CR path across the detector, finds out if nearby pixels are crossed and then follows the energy cascade. All energy lost through ionization is converted into electrons detected by the readout chain, their number being given by the ratio between the total energy loss in each pixel and the minimal ionization energy (i.e. the long-wavelength cutoff energy). Once the charge released in each pixel has been estimated, the inter-pixel capacitive coupling is taken into account. This can be done in two ways. The easy one is to multiply the pixels affect by CR by a factor

$$\alpha = \frac{V_c}{V_0 + 4V_c} \tag{1.5}$$

where V_0 is the voltage of the central pixel, affected by the cosmic ray, and V_c is the capacitive voltage appearing at the four adjacent pixels. The capacitive coupling is expressed by the relation:

$$V_c = \frac{\frac{1}{C_0}}{\frac{1}{C_0} + \frac{1}{C_c}} V_0 \ . \tag{1.6}$$

One can typically assume $\alpha = 0.015$. With this filter, the central pixel is depressed by the a factor $4\alpha = 0.94$ (Fig.10).

	0.015	
0.015	0.94	0.015
	0.015	

Figure 10: basic IPC filter assuming $\alpha = 0.015$ and 4 pixel coupling.

In fact, one should take into account that the coupling involves, in principle, more than the 4 adjacent pixels. This may be important for the most energetic events, which can have capacitive effects noticeable at distances larger than the immediately adjacent pixels. Instead of solving a complex network system, one can more simply notice that the 2nd next pixel must be coupled to the central one by a factor close to α^2, the third pixel by a factor α^3, and so on. Along this line, one can imagine to convolve the original CR signal with a filter function given by

$$F(x,y) = \alpha^{d(x,y)} \tag{1.7}$$

where $d(x,y)$ is the distance from the central pixel. We use this filter function, properly normalized to preserve the flux. Its values are shown in Figure 11, for the inner 5x5 pixels.

6.470E-6	7.786E-5	0.0002	7.786E-5	6.470E-6
7.786E-5	0.00245	0.1399	0.00245	7.786E-5
0.0002	0.1399	0.0932	0.1399	0.0002
7.786E-5	0.00245	0.1399	0.00245	7.786E-5
6.470E-6	7.786E-5	0.0002	7.786E-5	6.470E-6

Figure 11: IPC filter function, assuming $\alpha = 0.015$, *for the 5×5 inner pixels.*

Figure 12 shows 9 typical results, calculated for a HgCdTe detector with 5.5micron cutoff wavelength. All figures refer to protons of increasing energy, with the exception of the last 2 which refer to Helium nucleons. Figure 12 clearly illustrates that the amount of energy deposited by a CR in a pixel does not depend only by the energy of the CR itself

(see e.g. the large difference between the first two events occurring at similar energy, 20.59MeV and 21.31MeV) but also on the amount of material crossed by the CR, i.e. ultimately on the CR direction.

A total of 60,000 CR events have been produced. The naming convention and contents of the data files are discussed in Appendix 2.

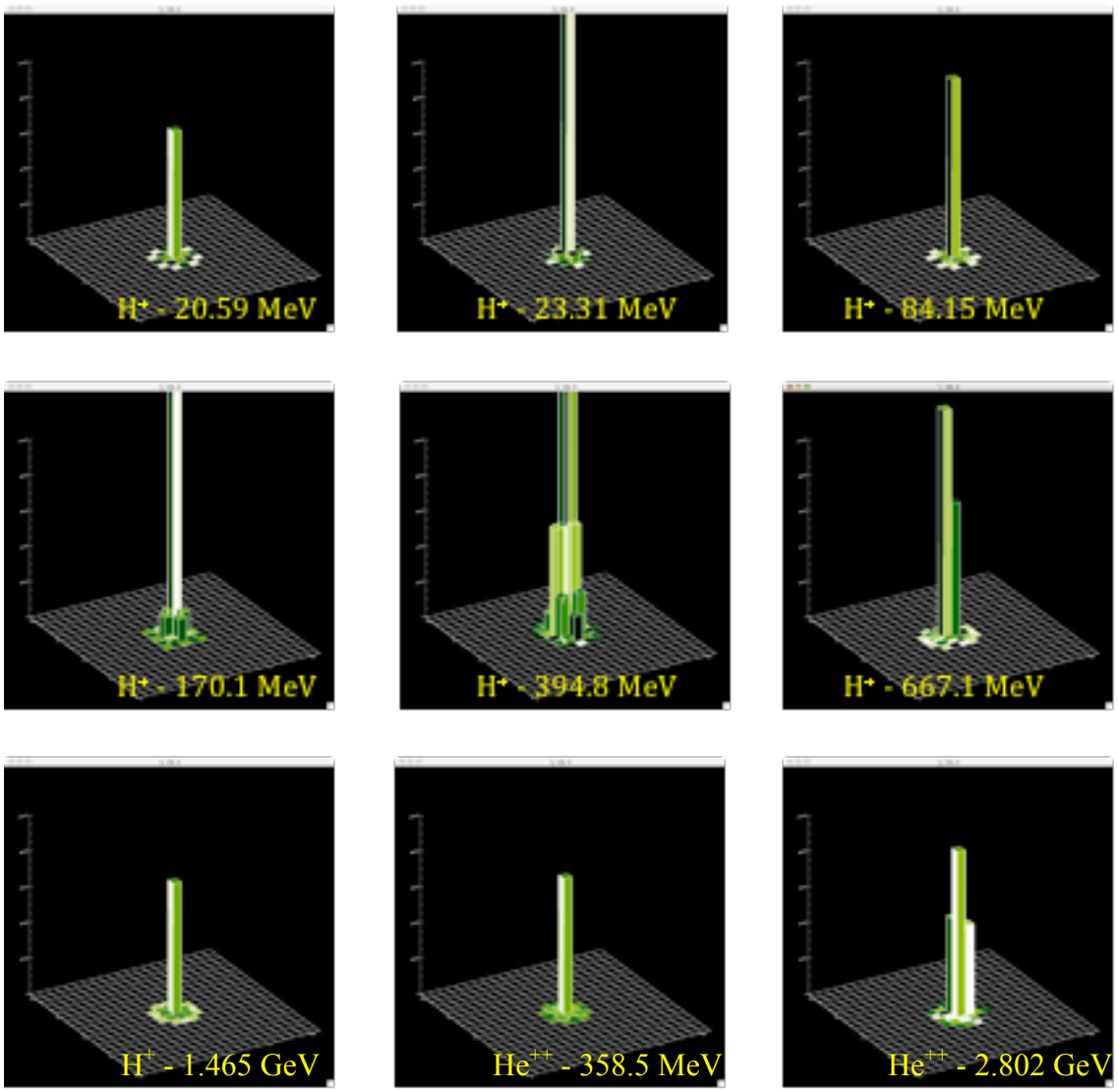

Figure 12: simulated CR events in 2.5micron HgCDTe detectors, for various energy, H and He nucleons

8.0 Conclusions

This document describes the derivation of a library of simulated cosmic ray events as seen by JWST HgCdTe detectors. The cosmic rays have been calculated assuming a spacecraft at L2 (i.e. about 1AU of distance from the Sun, no trapped particles), for different levels of solar activity, and taking into account the relative frequency of the

most abundant nucleons (H, He, C, N, O, Fe) together with their energy. A shielding of 100mil Al equivalent thickness has assumed. The cosmic rays have been traced through the detector material assuming they impact a random point within a pixel and are isotropically distributed. The energy losses have been calculated using state of the art modeling, taking into account the stoichiometric ratio and density of different types of HgCdTe and assuming optimal detector thickness. The effects of interpixel coupling has been included, whereas all other detector effects (e.g. readout noise, dark current, etc.) remain to be added.
In a future paper we will compare our predictions with the results obtained with WFC3 (on low earth orbit) and Deep Impact (which flew with a WFC3-like 1.7micron detector) to validate our assumptions.

9.0 References

Barth, J. L. & Isaacs J. C., "The Radiation Environment for the Next Generation Space Telescope", NGST Doc. 570 (1999)

Barth, L. "The radiation environment for the NGST", September 2000

Capper, P., in "Properties of narrow gap cadmium-based compounds", P. Capper Editor,. Series: EMIS Data Reviews. No. 10. (INSPEC/lnstitution of Electrical Engineers August).

Fodness, B., "Simulations of Radiations effects on NGST", Feb. 2002

Hansen, G. L., and Schmit, J. L., *Jour. Appl. Phys.,* **54**, 1639 (1983):

Rauscher, R., Isaacs, J. C., Long, K, "Cosmic Ray Management on NGST 1: The Effect of Cosmic Rays on Near Infrared Imaging Exposure Times", STScI-NGST-R-0003A (2000)

Amsler C. *et al.* (Particle Data Group), Physics Letters **B667**, 1 (2008) (on the web at http://pdg.lbl.gov/2006/reviews/passagerpp.pdf)

APPENDIX 1

It may be useful to briefly remind how to evaluate the typical CR energies. An electron has a rest energy $m_e c^2 = 0.511$ MeV, whereas a proton, with a mass 1836 times higher, has a rest energy $m_p c^2 = 938.3$ MeV, i.e. about 1 GeV. When one refer to a CR of, say, 10MeV one refers to its kinetic energy. The total energy E_{tot} is the sum of kinetic and rest energy, thus the relation

$$E_{tot} = E_k + m_0 c^2 = \gamma m_0 c^2 \tag{1.8}$$

provides $\gamma = E_{tot} / m_0 c^2 = \left[10\text{MeV} + 938.3\text{MeV}\right] / 938.3\text{MeV} = 1.0106$, for a 10MeV proton. The velocity v of a 10 MeV proton, related to the γ factor by:

$$\gamma = \frac{1}{\sqrt{1 - \frac{v^2}{c^2}}} \tag{1.9}$$

is therefore $v = 0.141\, c$, or about 1/8 of the speed of the light. To reach velocities close within a few percent of the speed of the light protons must have kinetic energy in the GeV range.

APPENDIX 2

There final dataset contains 10 files for each configuration; their naming convention labels their content. Files are named, in general, CRs_MCT*wl_model_xx*.fits, where *wl=2.5* or *5.5* refers to the detector material, *model=SOLMIN, SOLMAX* or *FLARES* refers to the assumed CR spectrum and *xx=00,01,…09*, refers to the file number. Therefore

1. For the solar minimum one has the sets of 20 files:
   - CRs_MCTwl_SOLMIN_xx.fits (xx = 00, 01, …09)
   - CRs_MCTwl_SOLMIN_xx.fits
2. For the solar maximum one has
   - CRs_MCT5.5_SOLMAX_xx.fits
   - CRs_MCT2.5_SOLMAX_xx.fits
3. For the solar flares one has
   - CRs_MCT5.5_FLARES_xx.fits
   - CRs_MCT2.5_FLARES_xx.fits

Each file is a multiextension fits file structured as follows

- Extension 0 is void
- Extension 1 contains a datacube of 1000 cosmic ray images, [21,21,1000], in units of electrons
- Extension 2 contains a vector of 1000 integer values labeling the nucleon: 0=H, 1=He, 2=C, 3=N, 4=O, 5=Fe
- Extension 3 contains a vector of 1000 real values giving the CR energy in MeV.

The 10 files provide a total of 10,000 cosmic ray per configuration. This should be sufficient to sample the energy spectrum and expected morphology of the CRs. The number of CR to be injected on a detector for a given exposure time can be derived using the recipe presented at the end of Section 4.0.